Liu *et al. Journal of Translational Medicine* (2026) 24:475
https://doi.org/10.1186/s12967-026-07952-2

Journal of Translational Medicine

RESEARCH Open Access

Structural dynamics of microtubules in glioma: impact on macrophage M2 polarization and tumor cell heterogeneity

Xinyu Liu[1†], Xin Sun[2†], Ningning Yao[1], Shi Hua[1*] and Yucheng Lu[1*]

Abstract

Background Glioma is the most common malignant brain tumor, characterized by high heterogeneity and poor prognosis. Microtubule dynamics regulate tumor progression and immune escape; however, the prognostic significance of microtubule-associated genes in glioma and their immunological significance still lack systematic investigation.

Methods We integrated transcriptomic and clinical data from TCGA and CGGA cohorts to identify microtubule-associated genes with prognostic significance. A risk score (RS) model was established using Cox regression and validated in independent cohorts. Spatial transcriptomics and single-cell RNA sequencing were applied to characterize the expression patterns of candidate genes across glioma microregions and immune cell populations. Functional enrichment analysis, immune infiltration assessment, and drug sensitivity profiling were performed to explore the biological mechanisms and clinical implications of the RS model.

Results We identified 18 microtubule-associated genes that are significantly associated with glioma prognosis and constructed a three-gene RS model (PAFAH1B1, SNAPIN, and MAD1L1), which robustly predicts overall survival. Tumors with high-RS exhibited increased infiltration of M2 macrophages, enhanced immunosuppressive signaling, and reduced sensitivity to alkylating agents. Spatial and single-cell analyses confirmed that core RS genes are enriched at the tumor-immune interface and shaped macrophage polarization dynamics.

Conclusion Our findings highlight microtubule-associated genes as key regulators of the glioma immune microenvironment. The RS model serves as a clinically applicable biomarker for prognostication and therapeutic stratification, with potential implications for optimizing immunotherapy and chemotherapy strategies in glioma patients.

Keywords Microtubule dynamics, Glioma, M2 macrophage polarization, Spatiotemporal heterogeneity

[†]Xinyu Liu and Xin Sun contributed equally to this work and should be regarded as co-first authors.

*Correspondence:
Shi Hua
252900349@qq.com
Yucheng Lu
luyu-20@163.com
[1]Guangzhou University of Chinese Medicine, Linyi People's Hospital, Guangzhou, Guangdong 510405, China
[2]Linyi People's Hospital, Linyi University, Linyi 276000, China

Introduction

Glioma is the most common primary malignant tumor of the central nervous system, accounting for approximately 75% of all malignant brain tumors [1]. According to global cancer statistics, there are about 150,000 new cases annually, representing roughly 2% of all cancer diagnoses [2]. Among them, glioblastoma (GBM), classified as WHO grade IV, is the most aggressive type, with a dismal prognosis and a median survival of only 14.4 months [3–5]. The current standard of care includes maximal surgical resection, radiotherapy, and temozolomide (TMZ) chemotherapy [6, 7]. However, most patients experience recurrence within six months after surgery, and the recurrence rate of GBM approaches 100% [8, 9]. Due to pronounced molecular and cellular heterogeneity, resistance to TMZ and other chemotherapeutic agents is prevalent [10], severely limiting therapeutic efficacy. The fifth edition of the World Health Organization (WHO) classification of central nervous system tumors further emphasizes the prognostic significance of molecular biomarkers such as IDH mutation and MGMT methylation [11].

Despite these advances, reliable biomarkers capable of predicting therapeutic response and guiding personalized treatment strategies for glioma patients remain limited. Given that therapeutic resistance and immune evasion are closely intertwined in glioma, identifying biomarkers that simultaneously reflect tumor-intrinsic programs and immune context is of particular clinical relevance.

Beyond intrinsic tumor cell heterogeneity, glioma progression is profoundly influenced by a highly immunosuppressive tumor microenvironment (TME). Unlike many peripheral malignancies, gliomas are characterized by sparse lymphocyte infiltration and a predominance of myeloid-derived cells, particularly tumor-associated macrophages (TAMs), which may constitute up to 30–50% of the total tumor mass. Accumulating evidence indicates that TAMs in glioma preferentially acquire an M2-like, immunosuppressive phenotype, promoting tumor growth, angiogenesis, immune evasion, and resistance to therapy through the secretion of anti-inflammatory cytokines and suppression of cytotoxic T-cell activity [12, 13]. Importantly, TAM polarization is increasingly recognized as a dynamic and context-dependent process shaped by tumor-intrinsic programs and spatial cues within the glioma microenvironment. Recent studies suggest that noncanonical mechanisms, including cytoskeletal remodeling and cellular stress responses, may play critical roles in regulating macrophage functional states and sustaining an immunosuppressive niche [14]. These observations highlight the need to investigate tumor–immune interactions from a spatially and cellularly resolved perspective.

With advancements in sequencing technologies, there is an urgent need to identify novel biomarkers capable of predicting glioma patients' responses to chemotherapy, targeted therapy, and immunotherapy, thereby improving long-term clinical outcomes.

In recent years, cytoskeletal remodeling has been recognized as a central driver of tumor progression. The cytoskeletal network, composed of actin filaments, intermediate filaments, and microtubules, plays pivotal roles in cell proliferation, migration, and invasion [15–17]. Among these components, microtubules are particularly critical, as their highly dynamic assembly and disassembly govern essential processes such as cell division, differentiation, and signal transduction. Studies have demonstrated that microtubule dynamics in GBM are hijacked to promote aberrant proliferation, infiltration, and therapy resistance [18, 19]. For example, dysregulation of the γ-tubulin ring complex (γ-TuRC) leads to abnormal microtubule nucleation and chromosomal instability, thereby driving malignant progression [20]. Mutations in genes such as TUBA1A and TUBB3 disrupt microtubule architecture, further fueling tumorigenesis [21, 22]. Moreover, aberrations in microtubule-associated proteins (MAPs) and post-translational modifications (PTMs) markedly enhance the migratory and invasive capacities of glioma cells [23, 24]. Notably, beyond maintaining chromosomal segregation and intracellular transport, microtubules can also establish functional intercellular networks that mediate calcium signaling and organelle transfer, thereby bolstering glioma cell survival under stress or therapeutic pressure [25].

Microtubule heterodimers, composed of α- and β-tubulin, are the fundamental units of the cytoskeleton and are indispensable for maintaining cell morphology, mediating intracellular transport, and orchestrating spindle formation and chromosomal segregation during mitosis [26, 27]. Clinically, microtubule-targeting agents (MTAs), which disrupt microtubule dynamics to suppress tumor cell division, have demonstrated remarkable efficacy in the treatment of various cancers, such as paclitaxel and vinca alkaloids [28–30]. More recently, studies have revealed that post-translational modifications (e.g., acetylation) regulate microtubule stability and play a key role in cell migration [17]. In addition, novel microtubule-binding sites (e.g., the Tumabulin site) have been identified, providing potential targets for the development of next-generation anticancer agents [27]. Nonetheless, despite advances in other malignancies, the role of microtubule dynamics in glioma biology, remodeling of the immune microenvironment, and polarization of tumor-associated macrophages (TAMs) remains insufficiently understood.

In this study, we integrated multi-omics datasets, including bulk transcriptomics, single-cell

transcriptomics, and spatial transcriptomics, to systematically identify and validate key microtubule-related genes. Furthermore, we developed a microtubule-based risk score (RS) model and employed spatial and single-cell analyses to elucidate its role in glioma heterogeneity and immune remodeling.

Materials and methods

Transcriptome data acquisition and preprocessing

Transcriptomic data of glioma samples were obtained from The Cancer Genome Atlas (TCGA) and the Chinese Glioma Genome Atlas (CGGA), while transcriptomic profiles of normal cerebral cortex tissues were derived from the Genotype-Tissue Expression (GTEx) database. Samples lacking essential follow-up information (e.g., survival time, survival status, or pathological classification) were excluded. Batch effects were corrected and data were integrated using the SVA R package. Differential expression analysis was performed with the limma package, with significance thresholds set at $P < 0.05$ and FDR < 0.05.

Single cell transcriptome data analysis

Single-cell RNA sequencing (scRNA-seq) data were obtained from the CGGA database. Data preprocessing was conducted using the Seurat package, where low-quality cells were filtered out (detected genes < 100, UMI count < 50, or mitochondrial gene ratio > 5%). Principal component analysis (PCA) was applied for dimensionality reduction, and the JackStraw method was used to determine the optimal number of retained components. Clustering was performed with the Louvain algorithm based on the top 20 principal components, and cell-type annotation was achieved using the SingleR package. Subclusters were visualized using t-distributed stochastic neighbor embedding (t-SNE).

Pseudotime analysis was conducted with Monocle to reconstruct cellular developmental trajectories, while cell–cell communication networks were inferred using CellChat to explore intercellular signaling pathways.

Spatial transcriptomics data analysis

Spatial transcriptomic data were obtained from the GEO database. Quality control and batch effect correction were performed using the Seurat package, followed by nonlinear dimensionality reduction with UMAP. Cell subpopulations were identified using the Louvain algorithm and subjected to differential expression analysis. Based on annotations from SingleR, single-cell identities were mapped onto spatial transcriptomic sections, enabling visualization of their spatial distribution within tissue structures. Heatmaps generated with ggplot2 depicted the expression patterns of key genes across different spatial regions. Additionally, the MIAF (Microenvironment Immune Activation and Facilitation) method was applied to evaluate the spatial enrichment of immune cells within the tumor microenvironment.

Feature gene selection and functional enrichment

Gene Ontology (GO) enrichment analysis was performed to characterize the biological processes associated with differentially expressed genes (DEGs), while Kyoto Encyclopedia of Genes and Genomes (KEGG) annotation was used to identify glioma-related pathways. Functional enrichment was further conducted using the MSigDB database (c2.cp.kegg and c5.go gene sets), with thresholds of NOM $P < 0.05$ and FDR < 0.25. Subsequently, a random forest model was constructed using the randomForest package. The optimal number of trees was determined by minimizing cross-validation error, and feature genes were selected based on an importance score > 2. This step was designed to reduce dimensionality while retaining microtubule-related genes with the strongest predictive contribution.

To further refine candidate genes beyond functional enrichment, immune-related gene sets were incorporated as a biological filtering layer rather than to define canonical immune genes. Specifically, immune-associated signatures were obtained from the MSigDB database and intersected with prognostic microtubule-related genes identified from differential expression and survival analyses. This step aimed to retain genes at the interface of cytoskeletal regulation and immune context, thereby enhancing the biological interpretability of downstream analyses.

Construction of prognostic RS model

LASSO regression was applied to further minimize overfitting and to identify a parsimonious gene set suitable for robust risk score construction.Candidate genes identified from the random forest model were subjected to univariate Cox regression and least absolute shrinkage and selection operator (LASSO) regression to determine prognostic markers. Genes retained after LASSO regression, including PAFAH1B1, SNAPIN, and MAD1L1, demonstrated non-zero and stable regression coefficients across cross-validation and were therefore selected as core components for RS model construction.For each of the three genes, the corresponding regression coefficient (Coef), hazard ratio (HR), and 95% confidence interval (CI) were explicitly calculated and reported to ensure transparency and reproducibility of the model.A risk score (RS) model was constructed based on the expression levels and regression coefficients of these genes:

$$\mathrm{RS} = \sum (\mathrm{Exp_i} \times \mathrm{Coef_i})$$

Specifically, PAFAH1B1 exhibited positive coefficients (HR > 1), indicating their association with increased mortality risk, whereas MAD1L1 and SNAPIN showed a negative coefficient (HR < 1), suggesting a protective effect.

Each patient's RS was calculated and stratified into high- and low-risk groups according to the median value.

Survival analysis and clinical correlation

Kaplan–Meier survival curves for risk groups and feature genes were generated using the survminer package. Stratified analyses were conducted based on clinicopathological characteristics (e.g., tumor grade, age, and sex). A nomogram was constructed with the rms package, while forest plots and ROC curves were produced using the survival and timeROC packages to assess the model's independence and predictive performance.

Single-cell trajectory and annotation

Based on CGGA scRNA-seq data, glioma and macrophage (M1/M2) subtypes were annotated using curated marker sets. Monocle3 was applied to reconstruct cell differentiation trajectories, thereby mapping evolutionary pathways between tumor core and peripheral regions.

RS, immune infiltration, and macrophage polarization

The immune cell composition of tumor samples across risk groups was quantified using CIBERSORT, while 13 immune functions were evaluated via ssGSEA. Correlations between RS-related genes and immune cell populations—particularly M2 macrophages—were visualized with Corrplot and validated using Spearman's correlation tests. In addition, pan-cancer immune subtype classifications from the UCLA dataset were used to compare immune subtype distributions between high- and low-RS groups.

RS, immunotherapy, and chemotherapy sensitivity

Immunotherapy response data were obtained from the Imvigor210 cohort, enabling comparison of treatment outcomes (complete response, partial response, stable disease, and progressive disease) between high- and low-RS groups. Chemotherapy sensitivity data from the GDSC database were used to predict differential drug responses to common agents, including carmustine, irinotecan, cyclophosphamide, cisplatin, and temozolomide.

Statistical analysis

Comparisons between groups were conducted using Student's *t*-test or Wilcoxon rank-sum test, depending on data distribution. Survival differences were evaluated using the log-rank test. Statistical significance was defined as $P < 0.05$, with the following levels indicated: $p < 0.05$ (*), $p < 0.01$ (**), $p < 0.001$ (***), and $p < 0.0001$ (****).

Results

Identification and expression analysis of microtubule-related genes

RNA sequencing data of glioma and normal samples were downloaded from The Cancer Genome Atlas (TCGA) and the Genotype-Tissue Expression (GTEx) database. Differential expression analysis was performed using the R package *limma*, which identified a total of 6,102 differentially expressed genes (DEGs). The expression profiles of these DEGs between tumor and normal tissues are presented in Fig. 1A. Gene Ontology (GO) enrichment analysis revealed that 130 genes were significantly enriched in microtubule-related biological processes (Fig. 1B). Based on feature importance ranking (importance score), 18 key genes with an importance score greater than 2 were further selected (Fig. 1C). Finally, chromosomal localization analysis indicated that these genes were distributed across different chromosomes (Fig. 1D).

Construction, evaluation, and validation of the risk score (RS)

Gene expression data and corresponding clinical information were first subjected to univariate Cox regression and LASSO regression analyses (Fig. 2A–B). The results identified several high-risk genes, including PRC1, SNAPIN, CSPP1, MAD1L1, POLDIP2, CCT7, and CETN2. The model achieved optimal performance when the λ value was set to 3. After incorporating immune-related gene sets, three microtubule-associated genes—PAFAH1B1, SNAPIN, and MAD1L1-were ultimately selected for model construction. To balance prognostic relevance with model robustness and avoid overfitting, a stepwise feature-reduction strategy was applied. Candidate genes were prioritized based on prognostic significance and feature importance, and further filtered by LASSO regression to retain only genes with stable, non-zero coefficients. After incorporating immune-related gene sets as a biological prioritization layer, three microtubule-associated genes—PAFAH1B1, SNAPIN, and MAD1L1—were consistently retained and ultimately selected for RS model construction.

Based on these genes, we established an RS model and calculated the risk score for each patient. Patients were stratified into high- and low-risk groups according to the median RS. Kaplan-Meier analysis demonstrated that patients in the high-risk group had significantly poorer overall survival compared with those in the low-risk group (Fig. 2C–D, $p < 0.001$). Further single-gene survival analyses revealed that high expression of MAD1L1 and SNAPIN was associated with unfavorable prognosis, whereas high PAFAH1B1 expression correlated

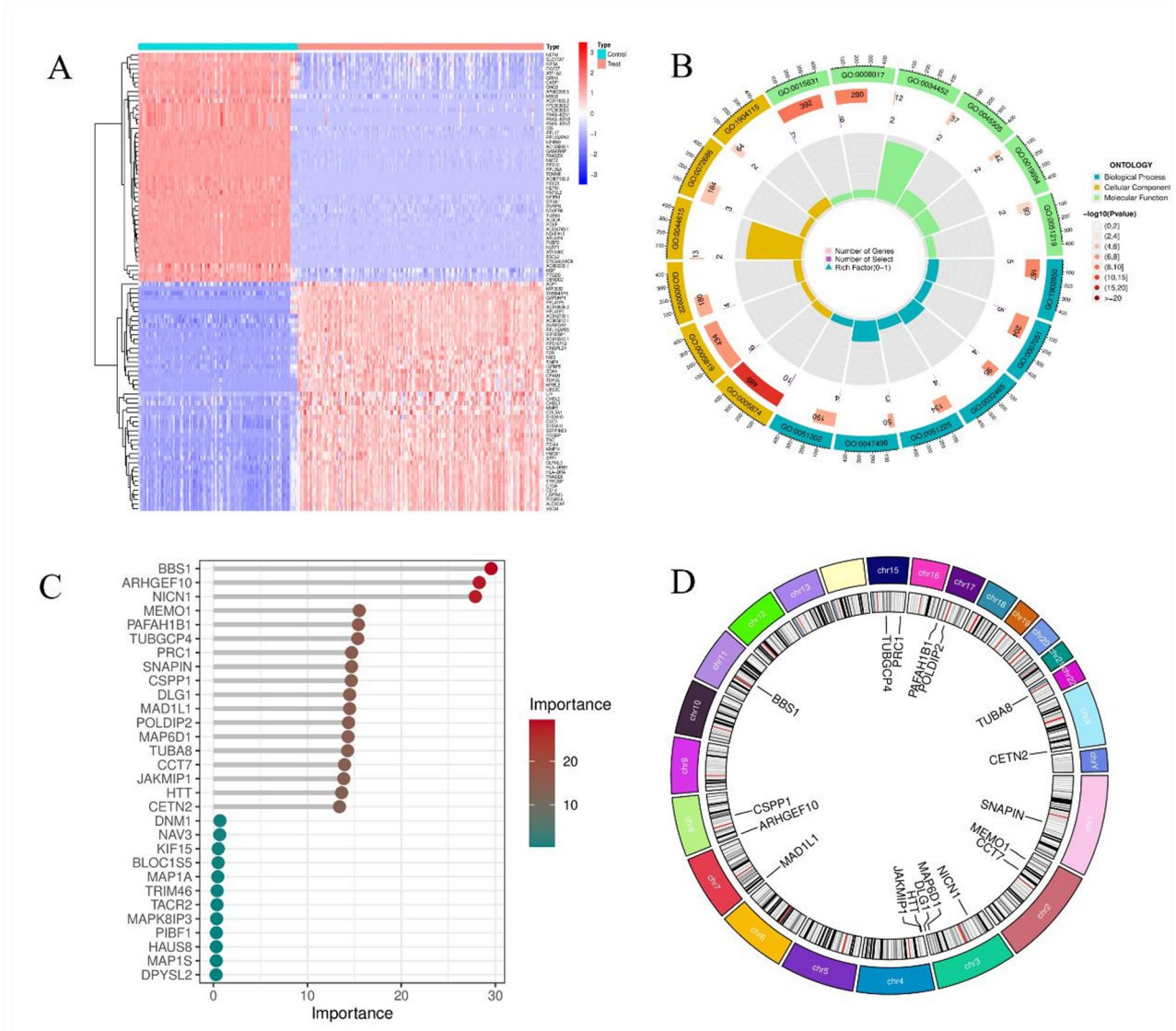

Fig. 1 Identification and characterization of microtubule-related genes in glioma. (**A**) Heatmap of 6102 differentially expressed genes between glioma and normal tissues. (**B**) GO enrichment highlighting 130 microtubule-related genes. (**C**) Feature importance ranking of candidate genes. (**D**) Chromosomal localization of 18 selected genes

with longer survival (Fig. 2E–G). A risk heatmap illustrated the expression patterns of the three genes across risk groups and their associations with clinical features, including grade, age, and diagnosis (Fig. 2H).

Multivariate Cox regression analysis indicated that age, grade, and RS were all independent prognostic factors (Fig. 2I). ROC curve analysis compared the predictive efficacy of the model with clinical features, revealing that the AUC value of RS (0.827) was superior to that of Age (0.783) and Gender (0.534) (Fig. 2J).

A nomogram integrating the RS and clinical parameters was then developed to predict 1-, 3-, and 5-year survival probabilities (Fig. 2K). Time-dependent ROC analysis demonstrated that the model achieved AUC values of 0.795, 0.825, and 0.827 at 1, 3, and 5 years, respectively, indicating robust and consistent predictive performance (Fig. 2L).

Value of RS in immunotherapy and chemotherapy

The predictive value of RS for immunotherapy outcomes was assessed in the IMvigor210 cohort. The results demonstrated that patients in the low-risk group had significantly lower survival probabilities compared to those in the high-risk group (Fig. 3A, $P = 0.030$). Response-based subgroup analysis further revealed that low-risk patients were more likely to achieve complete or partial response (CR/PR), whereas high-risk patients were more prone to stable disease or progressive disease (SD/PD) (Fig. 3B, $P = 0.0299$). Receiver operating characteristic (ROC) curve analysis indicated that the predictive performance

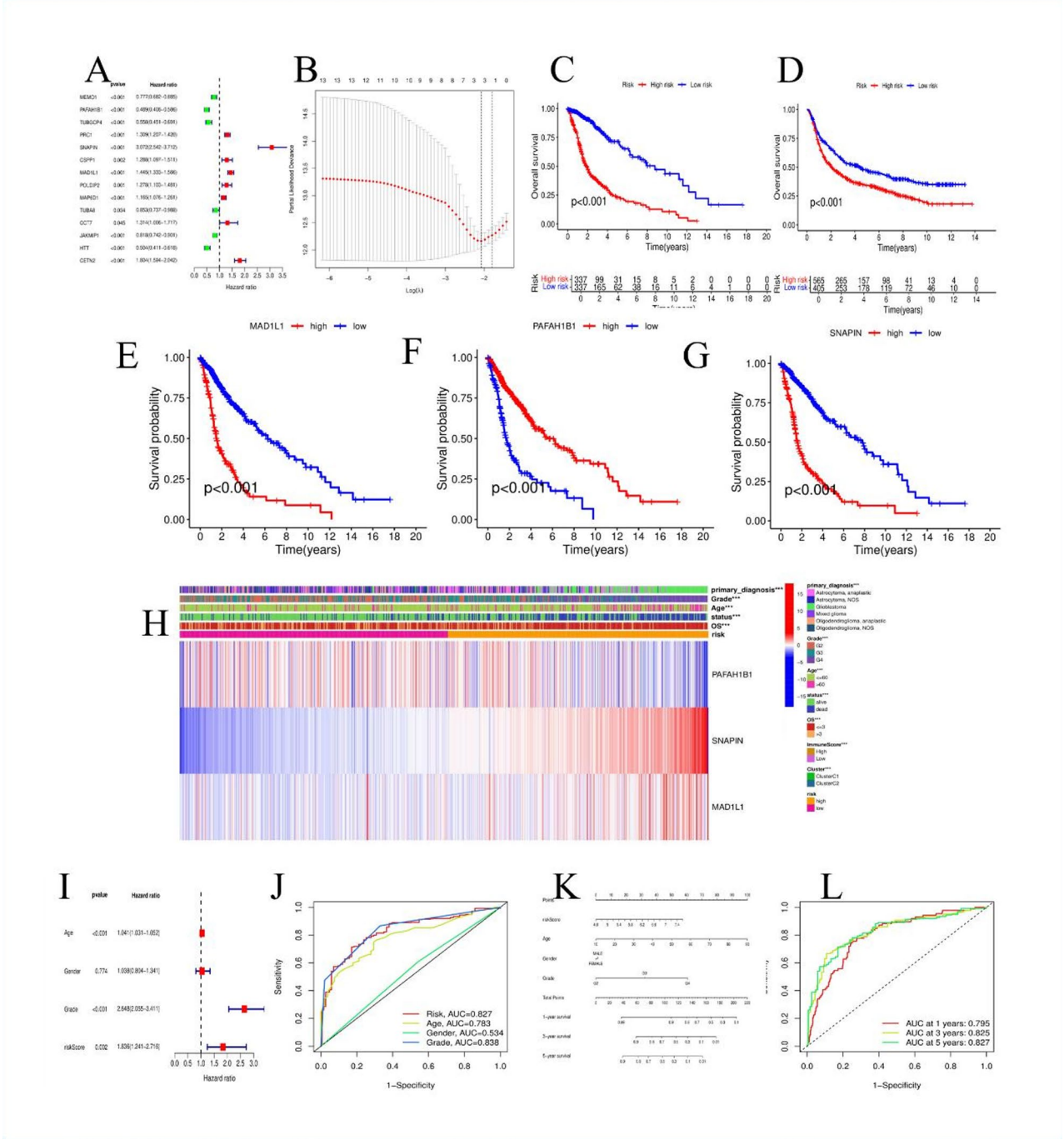

Fig. 2 Construction and validation of the RS model. (**A**-**B**) Feature selection using univariate Cox and LASSO regression. (**C**-**D**) Kaplan–Meier survival analysis of TCGA and CGGA cohorts stratified by RS. (**E**-**G**) Survival analysis of individual genes. (**H**) Heatmap integrating RS with clinical features. (**I**) Multivariate Cox regression of RS and clinical factors. (**J**) ROC curves comparing predictive performance. (**K**-**L**) Nomogram and time-dependent ROC validating survival prediction

of RS for immunotherapy response achieved an AUC of 0.619 (95% CI: 0.544–0.692) (Fig. 3C).

In the GDSC drug sensitivity analysis, no significant difference in sensitivity to irinotecan was observed between the two risk groups (Fig. 3D, $P > 0.05$). However, patients in the high-risk group were more sensitive to carmustine, cyclophosphamide, and temozolomide (Fig. 3E–G, $P < 0.05$), while those in the low-risk group were more sensitive to cisplatin (Fig. 3H, $P < 0.05$). In contrast, both groups exhibited resistance to vincristine and vinblastine, with no significant difference in response (Fig. 3I, $P = 0.9999$).

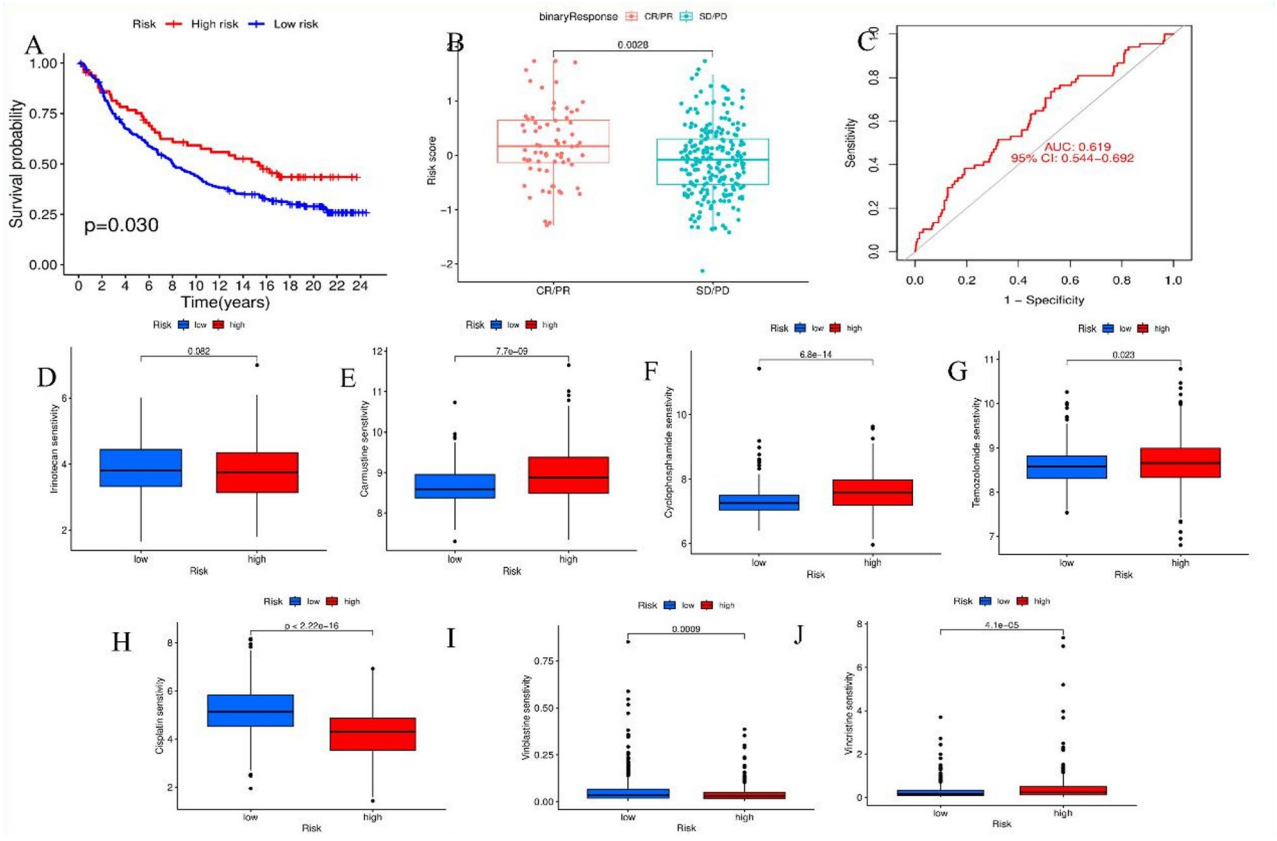

Fig. 3 Predictive value of the RS in immunotherapy and chemotherapy. (**A**-**C**) RS association with survival and response in the IMvigor210 cohort. (**D**-**G**) Drug sensitivity analysis showing RS-associated differences for alkylating agents. (**H**) Sensitivity of RS subgroups to cisplatin. (**I**-**J**) Lack of differential response to vincristine and vinblastine

Spatial transcriptomics reveals the correlation between key genes and malignant cell distribution in glioma microregions

Spatial transcriptomic analysis demonstrated that MAD1L1, PAFAH1B1, and SNAPIN exhibited heterogeneous expression across distinct glioma microregions and showed weak but statistically significant associations with the distribution of malignant cells.At the tumor–normal interface, all three genes displayed modest positive associations with malignant cell enrichment (Fig. 4A–C, MAD1L1: $r = 0.152$, $P < 0.01$; PAFAH1B1: $r = 0.182$, $P < 0.01$; SNAPIN: $r = 0.143$, $P < 0.01$).In the perivascular region, their expression levels were weakly yet consistently associated with malignant cell distribution (Fig. 4D-E, MAD1L1: $r = 0.100$, $P < 0.01$; PAFAH1B1: $r = 0.104$, $P < 0.01$; SNAPIN: $r = 0.146$, $P < 0.01$). In contrast, within the necrotic regions, MAD1L1 expression exhibited a weak negative association with malignant cells (Fig. 4G, $r = -0.071$, $P < 0.01$), whereas PAFAH1B1 and SNAPIN showed very weak but statistically significant positive associations (Fig. 4H-I, PAFAH1B1: $r = 0.034$, $P < 0.01$; SNAPIN: $r = 0.096$, $P < 0.01$).

Beyond malignant cell distribution, spatial expression maps further revealed that regions with high expression of MAD1L1, PAFAH1B1, and SNAPIN frequently overlapped with immune-influenced microenvironmental niches, particularly at the tumor–normal interface and within perivascular areas, whereas comparatively lower expression levels were observed in non-immune-dominant regions.

Taken together, although the observed correlations were modest in magnitude, their consistency across multiple spatial contexts supports a non-random spatial association between these genes and malignant cell localization. Importantly, these patterns likely reflect the non-linear and context-dependent nature of spatial transcriptomic relationships rather than direct or deterministic effects.

Spatial visualization further revealed that high-expression zones of these genes largely overlapped with malignant cell-enriched areas, while low-expression regions were mainly located in areas dominated by non-malignant cells. Together, these findings indicate that the spatial expression patterns of MAD1L1, PAFAH1B1, and SNAPIN are associated with malignant cell localization within immune-influenced microenvironmental regions rather than reflecting classical metastatic behavior.These findings provide direct spatial evidence linking gene

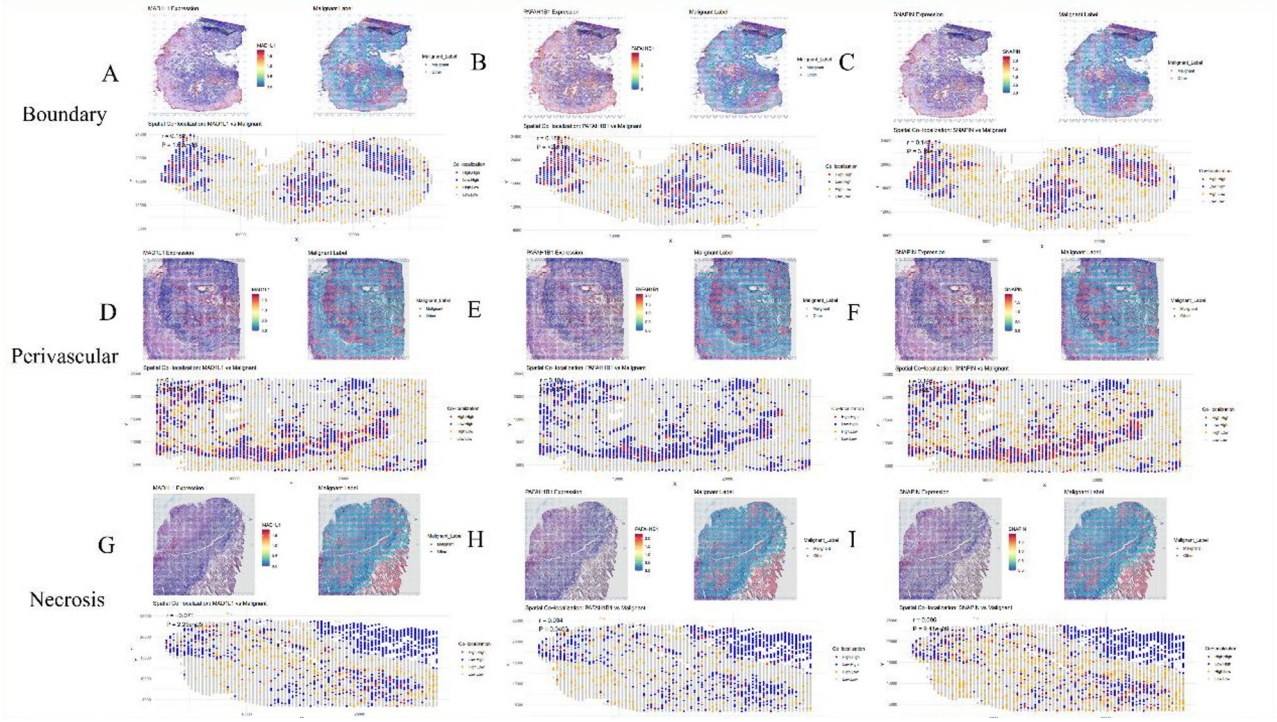

Fig. 4 Spatial expression patterns of microtubule-associated genes across glioma microregions. (**A**-**C**) Correlation of MAD1L1, PAFAH1B1, and SNAPIN with malignant cells At the tumor–normal interface. (**D**-**F**) Gene expression patterns in the perivascular region. (**G**-**I**) Spatial distribution of gene expression in necrotic areas

expression patterns with specific cellular distributions in glioma.

Identification and functional analysis of tumor immunity-related features

In the single-cell transcriptomic data from the CGGA cohort, UMAP visualization revealed the distribution of major cellular subpopulations, including astrocytes, macrophages, monocytes, and a small fraction of T cells (Fig. 5A). Further clustering analysis showed that macrophages could be subdivided into M1, M2, and other subgroups, among which the M2 population was markedly enriched (Fig. 5B). Pseudotime trajectory analysis demonstrated dynamic expression changes of the key genes during cell-state transitions: MAD1L1 and PAFAH1B1 expression gradually increased along pseudotime, whereas SNAPIN expression progressively decreased (Fig. 5C). Rather than representing static cell-type–specific markers, these temporal expression patterns suggest that the three genes are associated with continuous transitions of tumor and immune cell states. Consistently, UMAP scatter plots confirmed these findings, illustrating the distinct expression patterns of MAD1L1, PAFAH1B1, and SNAPIN across different cellular subpopulations, thereby validating their dynamic alterations along the pseudotime trajectory (Fig. 5D–G). Notably, their dynamic expression trends were particularly evident within macrophage subsets, supporting a potential association with macrophage polarization processes during glioma progression. Together, these findings highlight that the three genes may reflect functional dynamics within the tumor immune microenvironment, particularly during malignant progression and immune state remodeling, without implying a direct causal role.

The significance of RS in the tumor immune microenvironment

To investigate the potential association between the differentially expressed genes and immune-related processes, we performed KEGG enrichment analysis. The results showed that genes in the high-RS group were predominantly enriched in immune-related pathways, including antigen processing and presentation, cell adhesion molecules, cytokine–receptor interaction, ECM–receptor interaction, and focal adhesion (Fig. 6A).

Subsequently, CIBERSORT analysis was applied to evaluate the impact of RS on immune infiltration in gliomas. The findings revealed that M2 macrophages were predominant in the high-RS group, whereas monocytes were more abundant in the low-RS group (Fig. 6B). Furthermore, ssGSEA analysis demonstrated that differential expression of PAFAH1B1, SNAPIN, and MAD1L1 was significantly associated with the infiltration of 15

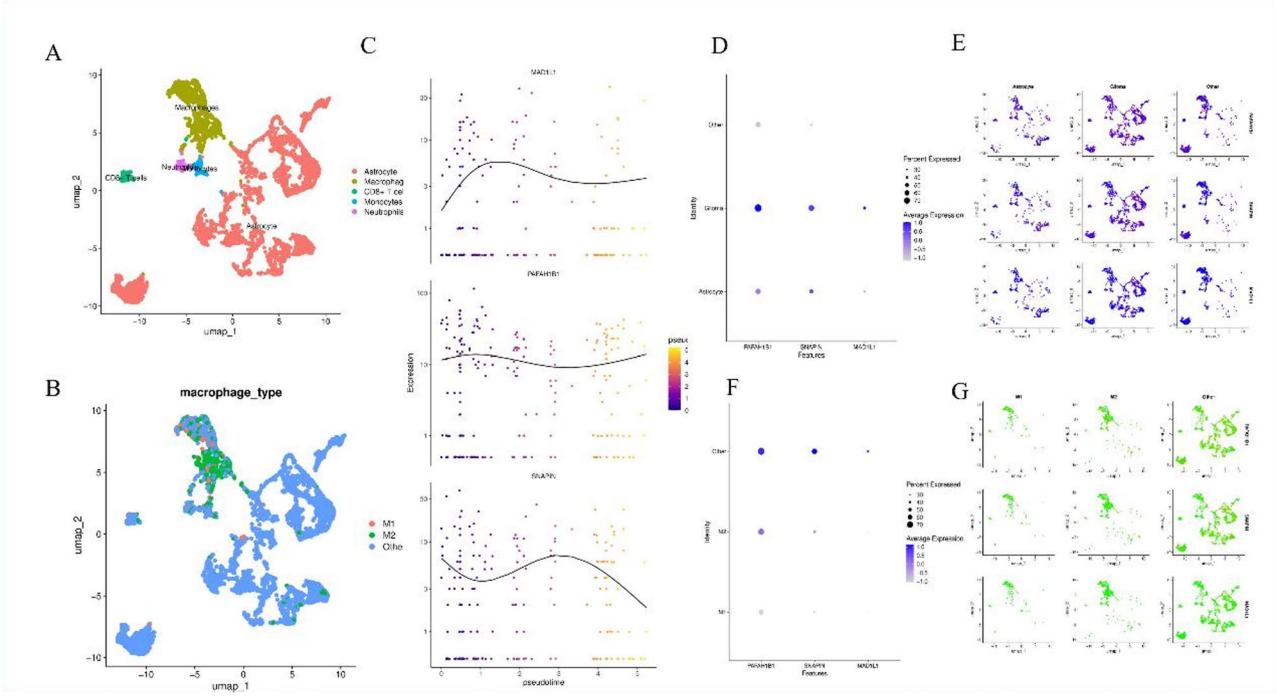

Fig. 5 Single-cell transcriptomics reveals immune-related signatures in glioma. (**A**) UMAP visualization of major glioma cell subpopulations. (**B**) Macrophage polarization trajectory toward the M2 phenotype. (**C**) Pseudotime expression dynamics of core genes. (**D**-**G**) Expression patterns of PAFAH1B1, SNAPIN, and MAD1L1 across glioma and macrophage subsets

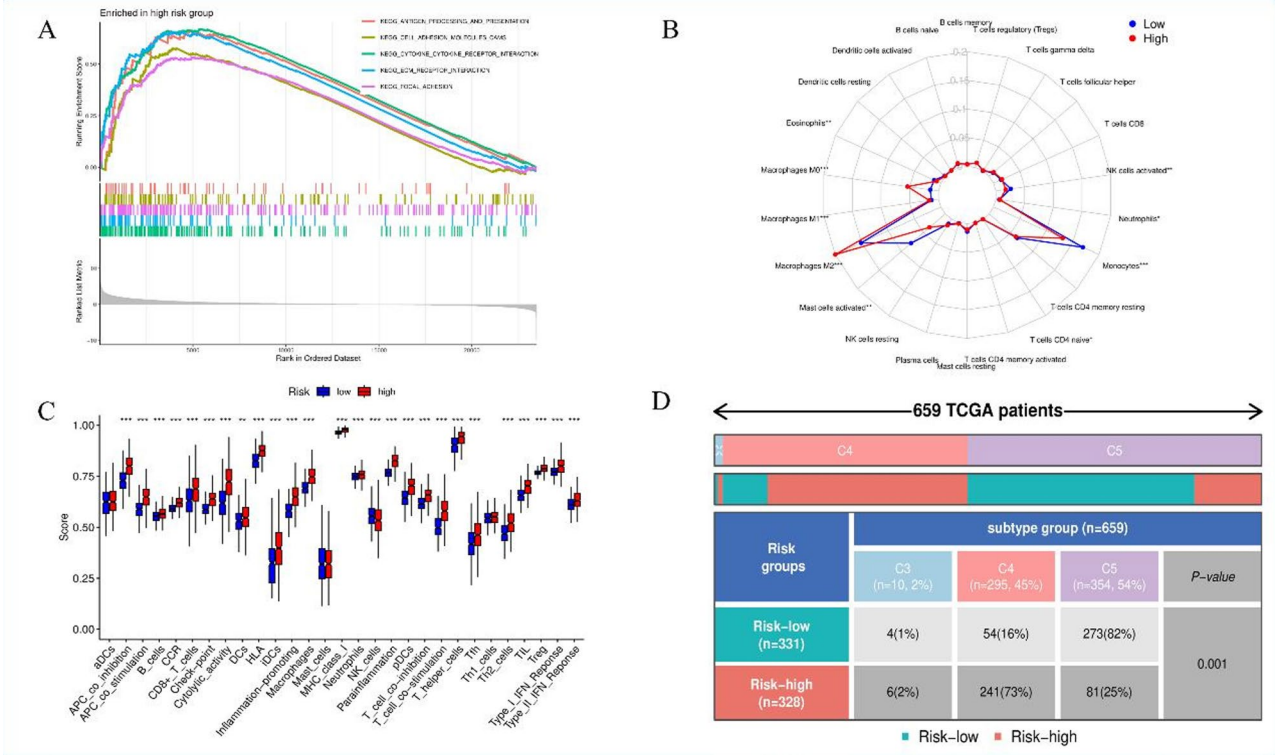

Fig. 6 Role of the RS in shaping the glioma immune microenvironment. (**A**) KEGG enrichment analysis of immune-related pathways. (**B**) CIBERSORT showing distinct immune infiltration patterns between RS subgroups. (**C**) ssGSEA linking gene expression with immune cell infiltration and functions. (**D**) Immune subtype distribution across RS groups in TCGA cohort

immune cell types and 13 immune-related functional signatures (Fig. 6C).

Finally, immune subtype analysis indicated a distinct distribution pattern between the two risk groups. Specifically, patients in the high-RS group were primarily enriched in the C4 lymphocyte-depleted subtype, whereas those in the low-RS group were more likely to belong to the C5 immunologically quiet subtype (Fig. 6D).

Discussion

Glioma is characterized by pronounced heterogeneity and an immunosuppressive microenvironment, which remain major barriers to effective therapy [31–34]. In this study, we systematically elucidated the central role of microtubule dynamics in glioma progression. By integrating multi-omics, spatial transcriptomics, and single-cell sequencing analyses, we identified three microtubule-associated signature genes (PAFAH1B1, SNAPIN, and MAD1L1) that are strongly correlated with glioma prognosis, and constructed a novel risk score (RS) model. Importantly, this RS model was designed not merely as a prognostic classifier, but as a biologically interpretable framework linking cytoskeletal regulation to immune remodeling and spatial heterogeneity within the tumor microenvironment (TME). This model not only outperformed conventional clinical parameters in predicting overall survival (OS), but also reflected distinct immunological features of the TME, providing insights into potential responses to chemotherapy and immunotherapy. Spatial and single-cell analyses further revealed marked spatiotemporal heterogeneity in the expression of these genes across tumor regions and cellular states, suggesting that they may influence glioma progression by regulating macrophage polarization and immune evasion.

Previously, extensive research on prognostic models for glioma has focused on extracellular matrix (ECM)-related features (MLDPS) and radiogenomics (MOFS) [35, 36]. While these models have improved prognostic stratification, most emphasize either stromal remodeling or imaging-derived features and largely overlook cytoskeletal dynamics as a driver of tumor–immune interactions. In contrast, this study is the first to incorporate microtubule dynamics into the prognostic prediction framework for glioma. By integrating immune-related gene sets as a biological prioritization layer, our RS model captures the intersection between microtubule regulation and immunosuppressive remodeling, rather than relying solely on immune abundance or ECM composition. While earlier research highlighted the roles of ECM remodeling and immune suppression, most models failed to capture the interplay between cytoskeletal dynamics and the immune microenvironment. Our RS model partially addresses this gap: on one hand, it demonstrated superior predictive accuracy (AUC up to 0.827); on the other hand, the spatial co-localization of SNAPIN with M2 macrophages, as well as the dynamic expression of PAFAH1B1 and MAD1L1 along differentiation trajectories, provides mechanistic interpretability that is often lacking in existing models. Thus, the novelty of this RS model lies not only in performance, but also in its capacity to link cytoskeletal regulation with immune polarization and spatial tumor ecology.

Based on univariate Cox regression analysis and Lasso regression analysis, we selected immunogenic microtubule genes from differentially expressed microtubule genes and identified three independent microtubule-related immune genes associated with prognosis. Among these genes, PAFAH1B1, SNAPIN, and MAD1L1 are all closely related to neurodevelopment and cell division stability. PAFAH1B1, a platelet-activating factor acetylhydrolase located on chromosome 17p13.3, whose mutations can lead to neuronal migration disorders [37, 38]; SNAPIN, as a regulatory factor of the SNARE complex, is involved in neuronal survival and neurotransmitter release. Its deficiency can result in reduced neuronal viability, degeneration, and central nervous system developmental defects [39, 40]; MAD1L1 is a core component of the spindle assembly checkpoint, and its structural abnormalities can cause mitotic errors and promote tumorigenesis [41, 42]. The convergence of these genes on cell division control and cellular stress adaptation may explain their association with aggressive glioma phenotypes and poor prognosis.

It is noteworthy that the RS demonstrated robust predictive power, highlighting its potential significance in prognostic assessment. Kaplan–Meier analysis revealed that the overall survival of patients in the high-risk group was significantly lower than that in the low-risk group. To comprehensively evaluate prognosis, we developed a nomogram incorporating various clinical parameters to score individual survival probability. Decision curve analysis (DCA) and concordance index (C-index) results indicated that the predictive accuracy of RS surpassed that of the traditional TNM stage. Furthermore, the nomogram integrating RS with clinical parameters (age, tumor grade) significantly improved prognostic predictive precision (1-/3-/5-year AUC: 0.89/0.85/0.83), supporting the added clinical value of RS beyond existing prognostic models.

Immune cells play pivotal roles in shaping the TME, thereby influencing tumor progression and treatment response. Glioma cells secrete inhibitory cytokines (e.g., IL-10, TGF-β), recruit regulatory T cells (Tregs) and tumor-associated macrophages (TAMs), and establish an immunosuppressive niche [43–46]. CIBERSORT, KEGG, and ssGSEA analyses indicated that the high-risk group

was characterized by marked infiltration of M2-type macrophages, whereas the low-risk group was dominated by monocytes. This aligns with findings by Wei et al., showing that M2-TAMs secrete IL-10 and TGF-β, recruit Tregs, and suppress T-cell activity, thereby driving immunosuppression [47]. The observed correlation between SNAPIN expression and M2 macrophage abundance further supports the notion that microtubule-associated genes may participate in immune polarization rather than acting as passive biomarkers. Moreover, immune subtype analysis indicated that high-risk patients were enriched in C4 (lymphocyte-depleted) tumors, whereas low-risk patients predominantly exhibited C5 (immunologically quiet) tumors, implicating microtubule genes as regulators of immune composition and activity [48, 49].

Regarding treatment prediction, the RS achieved comparable predictive performance for immunotherapy response in the IMvigor210 cohort (AUC = 0.619) relative to PD-L1 tumor proportion score (TPS) testing (KEYNOTE-024: AUC 0.65–0.70). Furthermore, our results highlighted associations between microtubule genes and chemotherapy sensitivity: high-risk patients were more responsive to carmustine, cyclophosphamide, and temozolomide, whereas low-risk patients showed greater sensitivity to cisplatin. These findings suggest that the RS may assist in therapeutic stratification, particularly in recurrent or temozolomide-resistant glioma.

Tumor heterogeneity manifests across patients, within distinct tumor regions, and over time, and is a hallmark of cancer biology [50, 51]. Highly heterogeneous tumors recruit non-malignant stromal cells (e.g., immune cells, fibroblasts, endothelial cells) to remodel the TME, producing spatial variations. This spatial distribution of malignant and stromal cells generates subregions with distinct microenvironments and functions, and is closely associated with poor prognosis [52–54]. Spatial transcriptomic analyses further emphasized the role of microtubule genes in glioma heterogeneity. PAFAH1B1, SNAPIN, and MAD1L1 exhibited region-specific expression patterns across the tumor–normal interface, perivascular niches, and necrotic zones, and their distribution correlated with malignant cell clusters. This spatially dependent expression suggests that microtubule dynamics not only regulate intracellular processes but also shape the ecological landscape of tumor subregions, potentially through interactions with immune cells [55, 56].

Single-cell RNA sequencing (scRNA-seq) provides a powerful approach to unravel transcriptomic features and intratumoral heterogeneity at single-cell resolution [57]. Initially reported by Tang et al. in 2009 [41], this technology enables quantitative profiling of gene expression, splicing, and allele-specific expression [58], and plays a critical role in dissecting drug-target pathways and tumor–TME interactions [59]. Compared with bulk RNA-seq, scRNA-seq offers the advantage of identifying cell-type-specific gene expression, annotating subpopulations, and reconstructing differentiation trajectories via computational methods [60, 61]. Applied to glioma and its TME, this facilitates precise localization of malignant cells, characterization of stromal interactions, and identification of aberrant expression patterns, thus informing therapeutic strategies and advancing our understanding of TME contributions to glioma progression [62]. Based on cellular trajectory analysis, this study projected glioma cells with different differentiation states into five distinct subpopulations, primarily including abundant astrocytes, immune infiltrates, macrophages, monocytes, and a small proportion of T cells. Further pseudotemporal analysis using the Monocle package revealed that SNAPIN gradually becomes inactivated during differentiation, while the expression of PAFAH1B1 and MAD1L1 progressively increases—consistent with their roles in cell survival, migration, and stemness maintenance [63]. These findings suggest a close association between glioma differentiation trajectories and immune regulation processes.

In summary, this study employed integrated multiomics, spatial, and single-cell analyses to construct a microtubule-based RS model. The model not only confirmed its value in prognosis prediction but also revealed associations with immunosuppressive TME characteristics and chemotherapy/immunotherapy responses. Future studies are warranted to validate the stability of the RS in larger clinical cohorts and to further explore therapeutic strategies targeting microtubule-associated genes to modulate the glioma immune microenvironment.

Nevertheless, several limitations should be acknowledged. This study is primarily based on integrative computational analyses, and although consistent evidence was obtained across bulk, single-cell, and spatial transcriptomic datasets, further experimental validation will be required in future studies to elucidate the causal mechanisms linking microtubule dynamics to immune remodeling and macrophage polarization in glioma.

Acknowledgements
Not applicable.

Author contributions
Xinyu Liu.: Conceptualization, Methodology, Writing – original draft; Writing – review & editing; Sun Xin and Ningning Yao: Data curation, Formal analysis; Writing – review & editing; Yucheng Lu and Shi Hua: Supervision, Funding acquisition, Writing – review & editing. All authors reviewed and approved the final manuscript.

Funding
This work was supported by Shandong Provincial Natural Science Foundation, China (no. ZR2023MH292).

Data availability
The datasets analyzed for this study can be found in the following public repositories: The TCGA glioma datasets (LGG and GBM) were downloaded from the UCSC Xena browser (https://xenabrowser.net/datapages/). The CGGA validation datasets were obtained from the Chinese Glioma Genome Atlas (http://www.cgga.org.cn/). Single-cell RNA sequencing and spatial transcriptomic data were sourced from the Gene Expression Omnibus (GEO) under the accession numbers provided in the Methods section. All data generated or analyzed during this study are included in this published article and its supplementary information files.

Declarations

Ethical approval
The data used in this study were all sourced from public databases such as TCGA and CGGA, and were all de identified public data. Therefore, this study does not require review and approval from the institutional ethics committee. All data processing strictly complies with relevant data usage agreements to protect patient privacy.

Consent for publication
Not applicable.

Competing interests
The authors declare no competing interests.

Received: 14 October 2025 / Accepted: 22 February 2026
Published online: 28 February 2026

References

1. Finch A, Solomou G, Wykes V, et al. Advances in research of adult gliomas. Int J Mol Sci. 2021;22(2):924.
2. Bray F, Laversanne M, Sung H, et al. Global cancer statistics 2022: GLOBOCAN estimates of incidence and mortality worldwide for 36 cancers in 185 countries. CA Cancer J Clin. 2024;74(3):229–63.
3. Louis DN, Perry A, Wesseling P, et al. The 2021 WHO classification of tumors of the central nervous system: a summary. Neuro Oncol. 2021;23(8):1231–51.
4. D'Amico AG, Maugeri G, Vanella L, et al. Multimodal role of PACAP in glioblastoma. Brain Sci. 2021;11(8):994.
5. Jiang T, Mao Y, Ma W, et al. CGCG clinical practice guidelines for the management of adult diffuse gliomas. Cancer Lett. 2016;375:263–73.
6. Tan AC, Ashley DM, López GY, et al. Management of glioblastoma: State of the art and future directions. CA Cancer J Clin. 2020;70(4):299–312.
7. Devleeschouwer S, Bergers G, Glioblastoma. To target the tumor cell or the microenvironment? Cancer J. 2017;23(2):74–82.
8. Thakur A, Faujdar C, Sharma R, et al. Glioblastoma: current status, emerging targets, and recent advances. J Med Chem. 2022;65(13):8596–685.
9. Oh T, Kaur G, Madden M, Bloch O, Parsa AT. Pleomorphic xanthoastrocytomas: Institutional experience of 18 patients. J Clin Neurosci. 2014;21(10):1767–72.
10. Bruford EA, Braschi B, Denny P, et al. Guidelines for human gene nomenclature. Nat Genet. 2020;52(8):754–8.
11. Cash AD, Aliev G, Siedlak SL, et al. Microtubule reduction in Alzheimer's disease and aging is independent of tau filament formation. Am J Pathol. 2003;162(5):1623–7.
12. Ke H, Li P, Li Z, et al. Immune profiling of the macroenvironment in colorectal cancer unveils systemic dysfunction and plasticity of immune cells. Clin Transl Med. 2025;15(2):e70175.
13. Ke H, Li Z, Li P, et al. Dynamic heterogeneity of colorectal cancer during progression revealed clinical risk-associated cell types and regulations in single-cell resolution and spatial context. Gastroenterol Rep (Oxf). 2023;11:goad034.
14. Liu J, Su Y, Zhang C, et al. NCOA3 impairs the efficacy of anti-PD-L1 therapy via the HSP90α/EZH2/CXCL9 axis in colon cancer. Int Immunopharmacol. 2025;155:114579.
15. Hempen B, Brion JP. Reduction of acetylated α-tubulin immunoreactivity in neurofibrillary tangle-bearing neurons in Alzheimer's disease. J Neuropathol Exp Neurol. 1996;55(9):964–72.
16. Matsuda W, Furuta T, Nakamura KC, et al. Single nigrostriatal dopaminergic neurons form widely spread and highly dense axonal arborizations in the neostriatum. J Neurosci. 2009;29(2):444–53.
17. Parker AL, Teo WS, McCarroll JA, Kavallaris M. An emerging role for tubulin isotypes in modulating cancer biology and chemotherapy resistance. Int J Mol Sci. 2017;18(7):1434.
18. Parker AL, Kavallaris M, McCarroll JA. Microtubules and their role in cellular stress in cancer. Front Oncol. 2014;4:153.
19. Dráber P, Dráberová E. Dysregulation of microtubule nucleating proteins in cancer cells. Cancers (Basel). 2021;13(22):5638.
20. Belvindrah R, Natarajan K, Shabajee P, et al. Mutation of the α-tubulin Tuba1a leads to straighter microtubules and perturbs neuronal migration. J Cell Biol. 2017;216(8):2443–61.
21. Tischfield MA, Baris HN, Wu C, et al. Human TUBB3 mutations perturb microtubule dynamics, kinesin interactions, and axon guidance. Cell. 2010;140(1):74–87.
22. Pienkowski T, Kowalczyk T, Cysewski D, et al. Glioma and post-translational modifications: A complex relationship. Biochim Biophys Acta Rev Cancer. 2023;1878:189009.
23. Škarková A, Pelantová M, Tolde O, et al. Microtubule-associated NAV3 regulates invasive phenotypes in glioblastoma cells. Brain Pathol. 2025;35(1):e13294.
24. Weil S, Osswald M, Solecki G, et al. Tumor microtubes convey resistance to surgical lesions and chemotherapy in gliomas. Neuro Oncol. 2017;19(10):1316–26.
25. Nogales E, Wolf SG, Khan IA, et al. Structure of tubulin at 6.5 Å and location of the taxol-binding site. Nature. 1995;375(6530):424–7.
26. Li Y, Zhang C, Tang D, et al. Identification of a ligand-binding site on tubulin mediating the tubulin–RB3 interaction. Proc Natl Acad Sci U S A. 2025;122(11):e240345122.
27. Sève P, Reiman T, Dumontet C. The role of betaIII tubulin in predicting chemoresistance in non-small cell lung cancer. Lung Cancer. 2010;67(2):136–43.
28. Ezzo M, Etienne-Manneville S. Microtubule-targeting agents: Advances in tubulin binding and small molecule therapy for gliomas and neurodegenerative diseases. Int J Mol Sci. 2025;26(14):7652.
29. Coulup SK, Georg GI. Revisiting microtubule targeting agents: α-Tubulin and the pironetin binding site as unexplored targets for cancer therapeutics. Bioorg Med Chem Lett. 2019;29(15):1865–73.
30. Yoshimoto S, Morita H, Okamura K, et al. αTAT1-induced tubulin acetylation promotes ameloblastoma migration and invasion. Lab Invest. 2022;102(1):80–9.
31. Sobue K, Toyoshima I, Iwasa K, et al. Non-neuronal microtubule-associated proteins are expressed in astrocytic gliomas of various phenotypes. Neurosurgery. 1989;25(5):690–8.
32. Nager M, Bhardwaj D, Canti C, et al. βIII-tubulin, a cytoskeletal protein, as a biomarker for glioblastoma: Implications for patient prognosis and therapy. Neuro Oncol. 2014;16(7):846–59.
33. Wang H, Xu T, Wang S, et al. MAPRE1 is a potential biomarker associated with tumor immune infiltration in glioblastoma. Front Genet. 2021;12:713419.
34. Lin Y, Xu J, Lan H, et al. Microtubule plus-end tracking proteins and their roles in glioma progression. Cancers (Basel). 2023;15(4):1090.
35. Forth S, Kapoor TM. The mechanics of microtubule networks in cell division. J Cell Biol. 2017;216(6):1525–31. https://doi.org/10.1083/jcb.201612064.
36. Mitchison T, Kirschner M. Microtubule dynamics and nucleation. Annu Rev Cell Biol. 1984;1:27–54.
37. Ganser LR, Myong S. Methods to study RNA-protein interactions. Nat Rev Mol Cell Biol. 2020;21(10):543–58. https://doi.org/10.1038/s41580-020-0256-0.
38. Gao J, Aksoy BA, Dogrusoz U, et al. Integrative analysis of complex cancer genomics and clinical profiles using the cBioPortal. Sci Signal. 2013;6(269):pl1.
39. Tang Z, Li C, Kang B, et al. GEPIA: A web server for cancer and normal gene expression profiling and interactive analyses. Nucleic Acids Res. 2017;45(W1):W98–102.
40. Wang Q, Li M, Yang M, et al. Glioma immune atlas: An integrative resource for profiling tumor immune microenvironment. Cancer Cell. 2022;40(6):559–e5743.
41. Xu H, Li T, Wang Q, et al. Immune-related risk model construction for glioblastoma. Front Immunol. 2021;12:698699.
42. Wu T, Hu E, Xu S, et al. clusterProfiler 4.0: A universal enrichment tool for interpreting omics data. Innov (Camb). 2021;2(3):100141.
43. Barbie DA, Tamayo P, Boehm JS, et al. Systematic RNA interference reveals that oncogenic KRAS-driven cancers require TBK1. Nature. 2009;462(7269):108–12.
44. Hänzelmann S, Castelo R, Guinney J. GSVA: Gene set variation analysis for microarray and RNA-seq data. BMC Bioinformatics. 2013;14:7.

45. Geeleher P, Cox NJ, Huang RS. pRRophetic: An R package for prediction of clinical chemotherapeutic response from tumor gene expression levels. PLoS ONE. 2014;9(9):e107468.
46. Sun D, Wang J, Han Y, et al. scRNA-seq analysis pipeline for tumor heterogeneity exploration. Cancer Cell. 2021;39(6):701–e7175.
47. Cheng J, Zhang J, Han Y, et al. CellMarker: A manually curated resource of cell markers in human and mouse. Nucleic Acids Res. 2019;47(D1):D721–8.
48. Jin S, Guerrero-Juarez CF, Zhang L, et al. Inference and analysis of cell-cell communication using CellChat. Nat Commun. 2021;12(1):1088.
49. Cao J, Spielmann M, Qiu X, et al. The single-cell transcriptional landscape of mammalian organogenesis. Nature. 2019;566(7745):496–502.
50. Bergen V, Lange M, Peidli S, et al. Generalizing RNA velocity to transient cell states through dynamical modeling. Nat Biotechnol. 2020;38(12):1408–14.
51. Trapnell C, Cacchiarelli D, Grimsby J, et al. The dynamics and regulators of cell fate decisions are revealed by pseudotemporal ordering of single cells. Nat Biotechnol. 2014;32(4):381–6.
52. Yu G, Wang LG, Han Y, He QY. clusterProfiler: An R package for comparing biological themes among gene clusters. OMICS. 2012;16(5):284–7.
53. Liu CJ, Hu FF, Xia MX, et al. GSCALite: A web server for gene set cancer analysis. Bioinformatics. 2018;34(21):3771–2.
54. Mayakonda A, Lin DC, Assenov Y, et al. Maftools: Efficient analysis, visualization and summarization of MAF files from large-scale cohort-based cancer studies. Genome Res. 2018;28(11):1747–56.
55. Liberzon A, Birger C, Thorvaldsdóttir H, et al. The Molecular Signatures Database (MSigDB) hallmark gene set collection. Cell Syst. 2015;1(6):417–25.
56. Rosenthal R, McGranahan N, Herrero J, et al. DeconstructSigs: Delineating mutational processes in single tumors distinguishes DNA repair deficiencies and patterns of carcinogenesis. Nat Genet. 2016;48(6):552–60.
57. Charoentong P, Finotello F, Angelova M, et al. Pan-cancer immunogenomic analyses reveal genotype-immunophenotype relationships and predictors of response to checkpoint blockade. Cell Rep. 2017;18(1):248–62.
58. Malta TM, Sokolov A, Gentles AJ, et al. Machine learning identifies stemness features associated with oncogenic dedifferentiation. Cell. 2018;173(2):338–e35415.
59. Neftel C, Laffy J, Filbin MG, et al. An integrative model of cellular states, plasticity, and genetics for glioblastoma. Cell. 2019;178(4):835–e84921.
60. Richards LM, Whitley OKN, MacLeod G, et al. Gradient of developmental and injury response transcriptional states defines functional vulnerabilities underpinning glioblastoma heterogeneity. Nat Cancer. 2021;2(2):157–73.
61. Wang L, Babikir H, Müller S, et al. The phenotypes of proliferating glioblastoma cells reside on a single axis of variation. Cancer Discov. 2019;9(12):1708–19.
62. Qiu X, Mao Q, Tang Y, et al. Reversed graph embedding resolves complex single-cell trajectories. Nat Methods. 2017;14(10):979–82.
63. Suvà ML, Tirosh I. The glioma stem cell model in the era of single-cell genomics. Cancer Cell. 2020;37(6):630–6.

Publisher's note